ICAS PAPER No. 72-27

THE OPTIMUM CONFIGURATION AND THE OPTIMUM REENTRY TRAJECTORY OF SPACE SHUTTLE VEHICLES

by
Jiro Kondo, Professor and Yasuhiko Aihara, Associate Professor
University of Tokyo
Takashi Tani and Akira Onji, Senior Scientists
National Aerospace Laboratory
Tokyo, Japan

The Eighth Congress of the International Council of the Aeronautical Sciences

INTERNATIONAAL CONGRESCENTRUM RAI-AMSTERDAM, THE NETHERLANDS
AUGUST 28 TO SEPTEMBER 2, 1972

Price: 3. Dfl.

THE OPTIMUM CONFIGURATION AND THE OPTIMUM REENTRY TRAJECTORY OF SPACE SHUTTLE VEHICLES

Jiro KONDO and Yasuhiko AIHARA
University of Tokyo, Tokyo, Japan
and
Takashi TANI and Akira ONJI
National Aerospace Laboratory, Tokyo, Japan

SUMMARY

Aerodynamic problems of a space shuttle, combining an unmanned orbitor with reusable boosters are considered.

The essential feature of the reentry flight is that of aerodynamic heating. It was found that the optimum trajectory of a winged reentry vehicle includes a large part of steady flight at a large angle of attack. The aerodynamic heating of a body at high angle of incidence in a steady hypersonic flow is investigated, and the optimal shape corresponding to the minimum heat input in various flight conditions is obtained. Obviously there exists no single shape which will correspond to the minimum heat input for every flow condition. The body minimizing the total heat input for the course of the reentry is discussed.

I. Introduction

We shall consider a space shuttle of combining an unmanned orbitor with reusable boosters. Although there are many unsolved problems involved in the detailed systems design of the space shuttle of this type. We will restrict ourselves in the aerodynamic problems of the orbitor with lifting wing in the reentry stage.

The typical reentry trajectry is indicated in the diagram of Mach number versus Reynolds number of Fig. 1. It is found that the reentry trajectory is included in every type of flow regime, free molecular flow, slip flow and continum flow. However, the majority of the reentry flight is included in the region of continum flight when the duration of flight at various conditions is considered. Moreover the flow around the reentry body can be assumed as steady since the boundary layer quickly accommodate with the conditions of the outer flow, while the rate of change of the flight conditions at the reentry environment are relatively slow.

The essential feature of the reentry flight is that of aerodynamic heating. It was found that the optimum trajectory of winged reentry body include a large part of steady flight at a large angle of attack Fig. 2 [1]. We will investigate the aerodynamic heating of a body at high angle of incidence in a steady supersonic flow in detail. We shall also consider the optimal shape corresponding to the minimum aerodynamic heating in various flight conditions. Obviously there exists no single shape which will corresponds to the minimum heat input for each flow condition. We should select a body which minimize the total heat input for the total range of the reentry flight. However since the configuration of the reentry body influence the Aerodynamic characteristics of the orbitor, and then the flight trajector is influenced by the performance of the orbitor therefore we should consider the optimum shape together with the optimum trajectory to minimize the total heat input during the reentry flight.

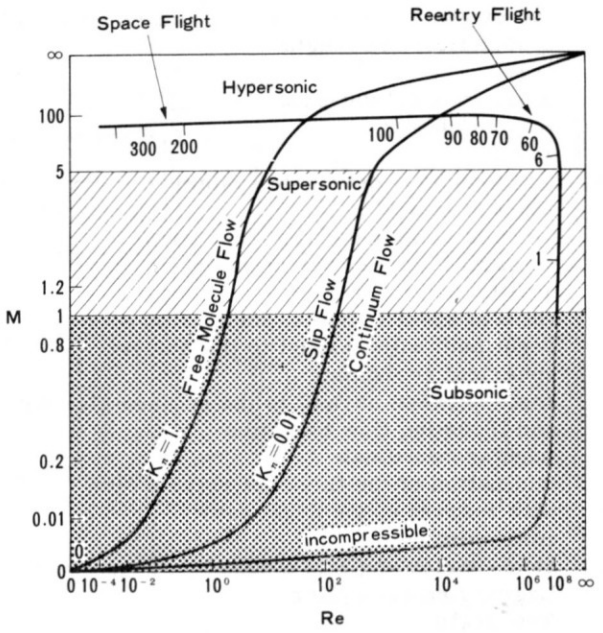

Fig. 1 Reentry Flight in Aerodynamic Regimes

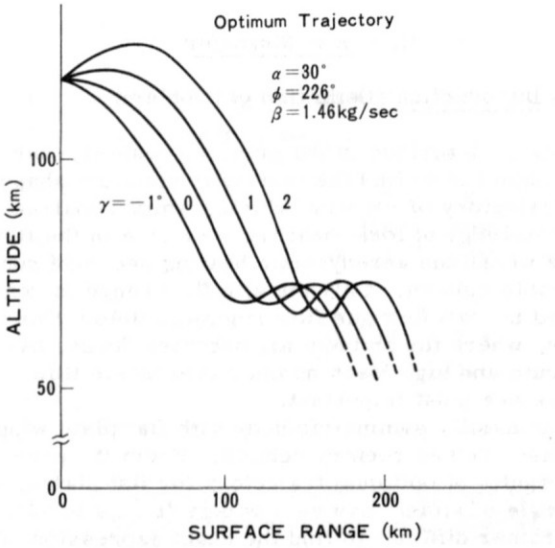

Fig. 2 Optimum Trajectories for Lifting Reentry

List of Symbols

c : exit velocity of retromotor
F : augmented function
g : gravity
g_* : gravity at sea level
h : heat transfer coefficient
I : objective function
Kn : Knudsen number
L : body length
V : volume
M : Mach number of the uniform flow
Pr : Prandtle number
P : pressure
local heat transfer rate cal/cm^2 sec
Q : Total heat transfer rate cal/sec
R_0 : radius at the stagnation point
R_B : base radius
Re : Reynolds number
s : arc length
s' : hypothetical arc length
S : area
t : time, integral variable
V : { volume of body / velocity
x, y, z : Cartesian coordinate system
α : angle of attack
$\bar{\alpha}$: thermal accommodation coefficient
β : mass flow rate of retro motor
heat transfer parameter
γ : ratio of specific heats, inclination of the flight path with respect to the horizon
θ : spherical coordinate
ψ : angle between normal to the surface element and incoming flow direction
ϕ : angular coordinate
ψ : inclination of the thrust of retro motor with respect to the flight path
φ_i : constraint
θ_c : semi-vertex angle of a cone
λ : Lagrangian multiplier
Λ : Yaw angle

II. Heat Transfer

2.1 Introduction (Definition of problem)

As is described in the previous chapter, our final object is to find the thermally optimum shape and trajectory of reentry behicle, which requires the knowledge of local heat transfer rate in the flow range where the aerodynamic heating becomes considerable amount. Only the slip flow range is concerned in rarefied gas flow regime. Below this range, where the ambient air becomes dense, hypersonic and high Mach number supersonic flow ranges are most important.

An axially symmetric body with flat plate wing is considered as reentry vehicle. From the previous results of optimum trajectory for flat plates,(1) the angle of attack may vary widely from 0 to 90°. It is rather difficult to find the exact expression of heat transfer rate at an arbitrary angle of attack even in the case of axially symmetric body.

In this chapter, therefore, approximate expression of heat transfer rate are introduced and discussed under several assumptions. Experimental studies are also conducted and the results confirm the validity of these approximate forms.

2.2 Rarefied gas flow

As for the heat transfer rate in hypersonic rarefied gas flow, studies are rather few and limited to the case of stagnation flow.(2)(3) We, therefore, tried to express this rate in simplified form for arbitrary bodies at an angle of attack.

In hypersonic rarefied flow regime the shock wave, if exists, is rather weak and simplified Newtonian flow model may well be adopted. According to this model, the normal velocity component of the incoming flow V_n disappears after it collides with the wall, while the tangential component remains unchanged. This loss of momentum is interpreted as the pressure at that point. It is well known that in the continuum hypersonic flow range, this simplified expression for pressure is fairly good approximation. Let us extend this concept to the energy-heat relation in rarefied flow regime. The incoming flow loses energy of $V_n^2/2$ per unit mass after collision. We assume that the heat transfered to the wall is proportional to this lost energy. Then, $\dot{q}_w$, the heat transfer rate at the wall can be written as follows;

$$\dot{q}_w = \frac{1}{2} C \rho V_n^2 \cdot V_n = \frac{1}{2} C \rho V_n^3$$

where C is independent of the local property. If we take so that at the stagnation point $\dot{q}_w$ coincides with that of Chow, C is a function of Re. For $V_n < 0$, we assume $\dot{q}_w = 0$

Let ψ be the angle between the surface normal and the flow direction, then $\dot{q}_w$ becomes

$$\dot{q}_w = (\dot{q}_w)_0 \cos^3\psi \quad \text{for } \cos\psi \geq 0 \quad (2.1),$$
$$\dot{q}_w = 0 \quad \text{for } \cos\psi < 0 \quad (2.2).$$

These simplified form enable us to calculate the total heat transfer rate for an arbitrary body at an

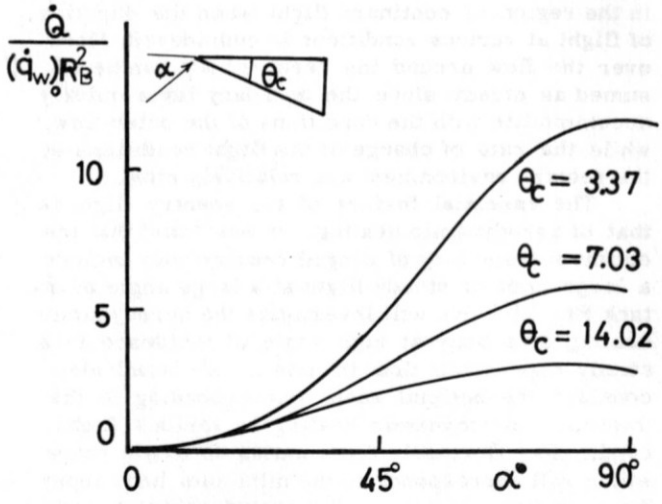

Fig. 3 Total heat transfer rate for half cone

angle of attack.

From the experiment described in the following section, the use of the simple Newtonian flow model in rarefied flow regime seems to be valid.

Calculated results for the half cone are shown in Fig. 3.

2.3 Rarefied gas flow experiment

The behavior of heat transfer in rarefied gas stream deviates from the results obtained for continuum flow and the characteristic phenomena such as free molecular effects and gas-surface interaction come up as important problems. Thus it is necessary for us to know some appropriate analytical methods having reasonable validity over a wide range of Knudsen number.

It is recognized that analysis based on Newtonian flow concept provides a convenient means not only in free molecular regime but also in high speed continuum flow field, which can be seen by the fact that the analytical results are in good agreements with measurements on aerodynamic characteristics of half cone as described in chapter 4.

As a contrastive example of wide validity of continuum flow analysis even in a high Knudsen number range, we refer to an experimental study performed at University of Tokyo on heat transfer from a two-dimensional circular platinum cylinder, 10 μ in diameter and 55 mm in length, in rarefied gas stream. The wind tunnel used for this study is shown in Fig. 4. This tunnel is a closed Goettingen type and is driven continuously at a given internal pressure within a range of 760 to 0.1 torr. The present experiment was conducted at internal pressures of 760, 200, 50, 30, 10, 5, 3, and 1.5 torr and at several wind velocities up to 20m/sec yielding the range of Reynolds number based on radius of the cylinder from 10 to 10^{-3}

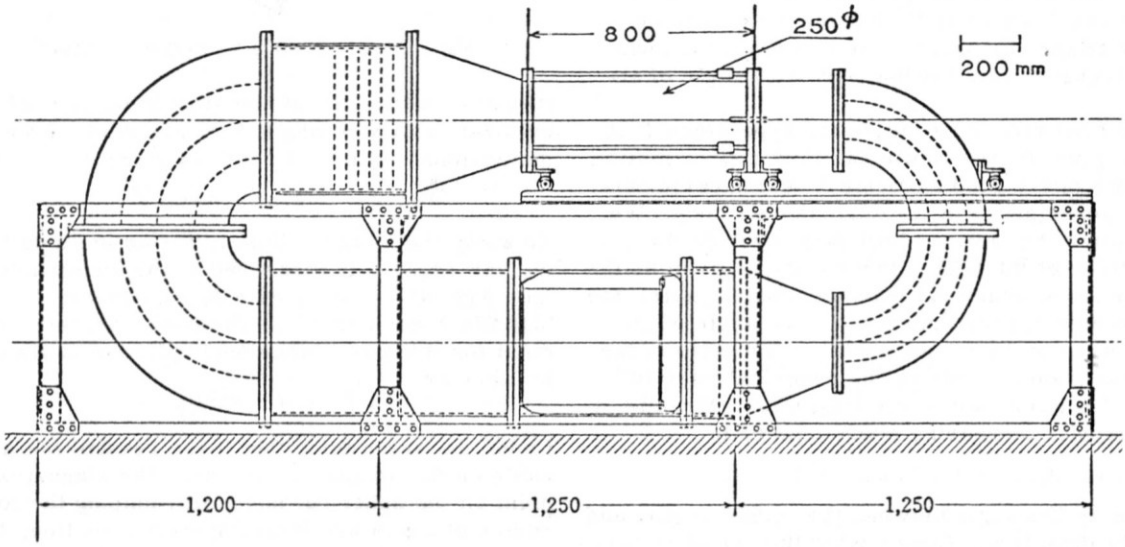

Fig. 4 Low density wind tunnel at University of Tokyo

and that of Knudsen number based on the same dimension from 10^{-2} to 6.14. The experimental scheme is almost the same as those in Refs. 4 and 5, and the details of the experiment will be published elsewhere.

One of the results is shown in Fig. 5. At Reynolds number of 10^{-2}, comparison is made for the analytical and experimental results in the form of Nusselt number vs. β where

$$\beta = \frac{2(2-\bar{\alpha})}{\bar{\alpha}} \frac{\gamma}{\gamma+1} \frac{K_n}{P_r}$$

provided that the temperature loading of the cylinder is small. (6) (7) The parameter derived from continuum flow analysis involves both Knudsen number Kn and thermal accommodation coefficient $\bar{\alpha}$, and thus it represents a combined molecular effect. Fig. 5 shows that continuum flow analysis explains the experimental results beyond the range of its application. This may be due to the characteristic feature that for large β the result of continuum

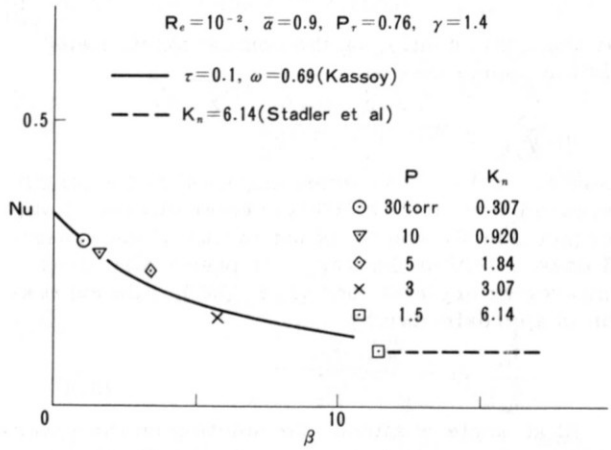

Fig. 5 Comparison of analytical and experimental results of Nusselt number vs. at Reynoldsnnumber of 10^{-2}. Working gas is air.

flow analysis approaches monotonically to that of free molecular flow analysis [8] without any contradiction, which also can be seen in Fig. 5. Though under these conditions as stated above of course we can not simulate the actual flight environment, it would be still necessary and instructive to collect such knowledges in order to develop some proper analytical method having wide application.

2.4 Hypersonic flow

The problem of aerodynamic heating of space shuttle at reentry flight becomes most serious at the hypersonic speed. Many studies have been presented for this problem, however, most solutions are only for two-dimensional or axially symmetirc body without angle of attack. For the purpose to calculate the optimum shape or optimum trajectory of minimum heat transfer, the simple analytical form of heat transfer coefficient about vehicle with angle of attack is desirable. We extend the result by Less [9] for the body without angle of attack, introduce a semi-empirical form of heat transfer rate for the body with angle of attack.

The pressure distribution for hypersonic flight speed is given by the Newtonian flow approximation, and shows fairly good agreement with experimental results especially for the blunt nosed body. We also assume the laminar boundary layer on the entire surface of the body. If the body is given by the combination of spherical nose and conical skirt, the heat transfer characteristics at zero angle of attack is given by Lees' theory [9]. The ratio of the local heat transfer rate on the spherical nose to the heat transfer rate at the stagnation point approaches with increasing Mach number to

$$\dot{q}_w/(\dot{q}_w)_0 = 1 - 0.722\ \theta^2 + \ldots.$$

where θ is the angle between the radius vector and the flight direction. Considering the result in rarefied flow regime (Sec. 2.2), we approximate this expression by the power of a trigonometric function

$$\dot{q}_w/(\dot{q}_w)_0 = (\cos\theta)^{1.44} \doteqdot \cos^{\frac{3}{2}}\theta. \qquad (2.3)$$

Far from the junction on the conical skirt, Lees' solution approaches to

$$\frac{\dot{q}_w}{(\dot{q}_w)_0} = \frac{(\sqrt{3}/2)\cdot\sin\theta_c\sqrt{\pi/2-\theta_c}}{\sqrt{s'/R_0}}$$

where θ_c is the semi-vertex angle, s' is the length measured from the hypothetic vertex of conical surface (see Fig. 6), and R_0 is the radius of the spherical nose. Within the range of practically used semi-vertex angle of cone ($0 \leqq \theta_c \leqq 30°$), this expression is approximated by

$$\frac{\dot{q}_w}{(\dot{q}_w)_0} \doteqdot \frac{\sin\theta_c}{\sqrt{s'/R_0}}. \qquad (2.4)$$

At an angle of attack, the solution on the spherical nose (2.3) also can be applied without any revise. The simplest approximation for conical skirt with an angle of attack is the solution for the inclined cylinder [10][11]. The ratio of the heat

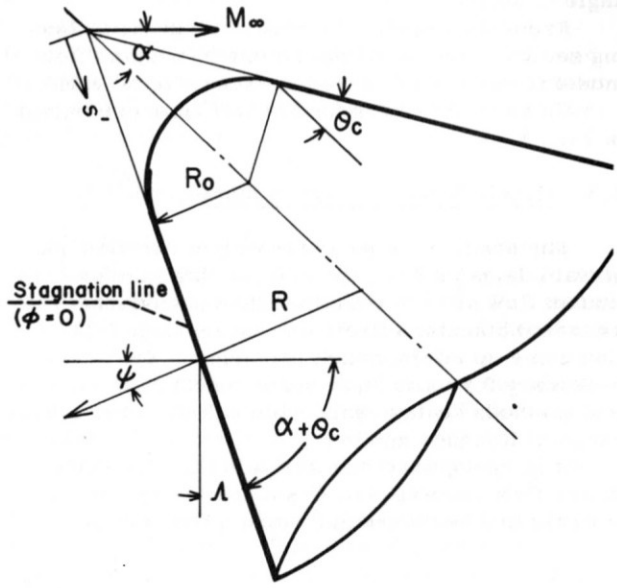

Fig. 6 Blunt cone at angle of attack

transfer coefficient at the stagnation line of the cylinder with yaw angle Λ to the value of the two-dimensional cylinder ($\Lambda = 0$) is given by

$$h_\Lambda / h_{\Lambda=0} \backsim (\cos\Lambda)^n$$

To apply this solution locally for an inclined cone, the yaw angle Λ is measured at the stagnation line (see Fig. 6). The power n approaches to 3/2 at high Mach number [10]. The heat transfer coefficient for the two-dimensional cylinder is also given by Lees as

$$h \backsim 1/\sqrt{R_0}$$

Under the assumption that these results are applicable on the stagnation line until the stagnation point on the spherical nose, introducing the local radius of curvature R on the stagnation line, the distribution of heat transfer rate is given by

$$\frac{\dot{q}_w}{(\dot{q}_w)_0} = \frac{\cos^{\frac{3}{2}}\Lambda}{\sqrt{R/R_0}} \doteqdot \frac{\cos^{\frac{3}{2}}\Lambda}{\sqrt{s'/R_0}\sqrt{\sin\theta_c}}. \qquad (2.5)$$

At the junction of the spherical nose and the conical skirt, $\Lambda = \theta$ and $R = R_0$, so this expression (2.5) coincides with (2.3). For the zero angle of attack, $\Lambda = \pi/2 - \theta_c$ and $\cos^{\frac{3}{2}}\Lambda = \sin^{\frac{3}{2}}\theta_c$, (2.5) coincides with (2.4)

Considering that the heat transfer rate becomes approximately zero at the zero value range of the Newtonian flow pressure distribution, we extend above result to circumferential distribution on the conical surface by

$$\frac{\dot{q}_w}{(\dot{q}_w)_0} = \frac{\cos^{\frac{3}{2}}\psi}{\sqrt{R/R_0}} \qquad (2.6)$$

where ψ is the angle between the normal of the surface element and the flight direction. We also define that (2.6) is valid only at the positive values, and otherwise becomes zero.

(2.6) is a semi-empirical expression of the

heat transfer rate on the blunt cone at an angle of attack. In the case of the cone-cylinder, (2.6) is also applicable locally for the cylindrical afterbody. At the junction of the conical nose and the cylindrical afterbody, causing by the rapid expansion of outer inviscid flow, a singularity appears in heat transfer rate distribution [12]. However this region with large heat transfer rate is limited and may be neglected for first approximation of the total integral of heat transfer on the entire surface. For the wing, the heat transfer rate can be estimated by the flat plate solution at an angle of attack. In this report, the interaction effect at the junction of the wing and the body is also neglected.

2.5 Hypersonic experimental results

Experimental results of the heat transfer on the body at an angle of attack in hypersonic flow are not so enough, and most of them are the results for the blunt cones [11][13][14]. In Fig. 7 we show the experimental data and analytical solution of Ref. 14 to compare with the expression (2.6) Our simple approximation is somewhat overestimate on the stagnation line ($\phi = 0$), however, shows generally good agreements with experimental data and the analytical solution.

For the cylindrical afterbody, the heat transfer has been measured in the N. A. L. hypersonic wind tunnel. The details of the wind tunnel are reported in Ref. 15. The model is a hemisphere-cylinder with a base diameter 80 mm (Fig. 8). Thermocouples were installed in its surface. The range of attack angle was restricted by the tunnel diameter, we could have the data only upto $\alpha = 25°$. The experiments are condected at $M_\infty = 7.1$, $Re = 3 \sim 10 \times 10^4/cm$, and these results show fairly good agreements with the estimation (2.6) (Figs. 9.a-9.b).

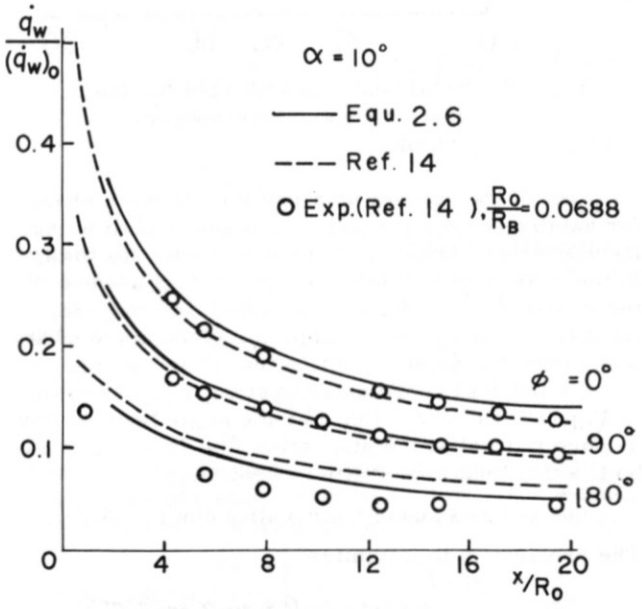

Fig. 7 Longitudinal variation of heat transfer on spherically blunted cone with 30° semi-vertex angle, at $M_\infty = 10.6$, $\phi = 0$, 90°, and 180°

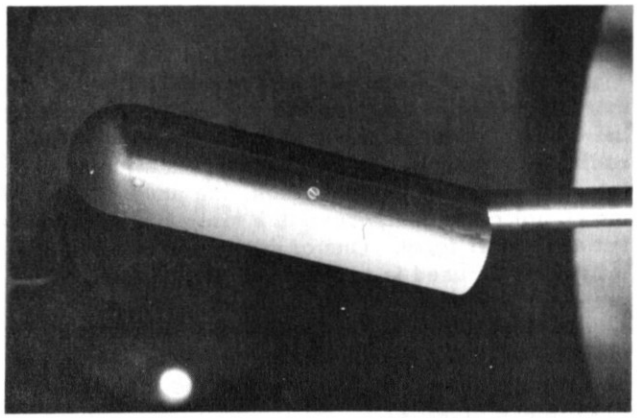

Fig. 8 Hemisphere-cylinder heat transfer model in N. A. L. hypersonic wind tunnel

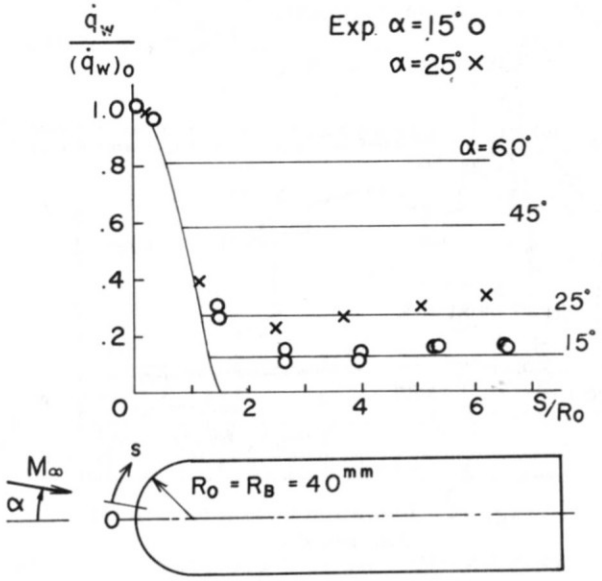

Fig. 9.a Longitudinal variation of heat transfer ratio on the stagnation line of a hemisphere-cylinder at $M_\infty = 7.1$

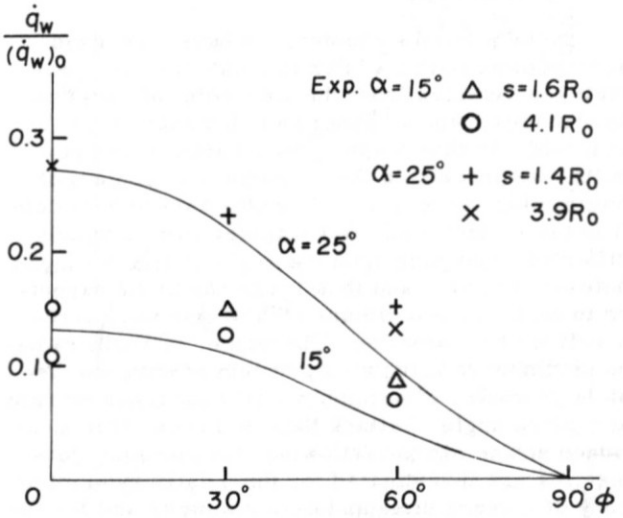

Fig. 9.b Circumferential variation of heat transfer ratio on a hemisphere-cylinder at $M_\infty = 7.1$

2.6 Radiation

With the increase of flight velocity, it is known that the radiative heat transfer becomes dominating the other processes in aerodynamic heating. As radiation is essentially due to the excitation of the internal modes of gas particles, the phenomena are too complicated to express in a simple and convenient analytical form. One of the approximation relatively wide used is to treat the gas as optically grey one.

In Ref. 16, however, a more realistic treatment by utilizing the radiation characteristics data of a nongrey gas (Fig. 10) is made and interesting results are obtained.

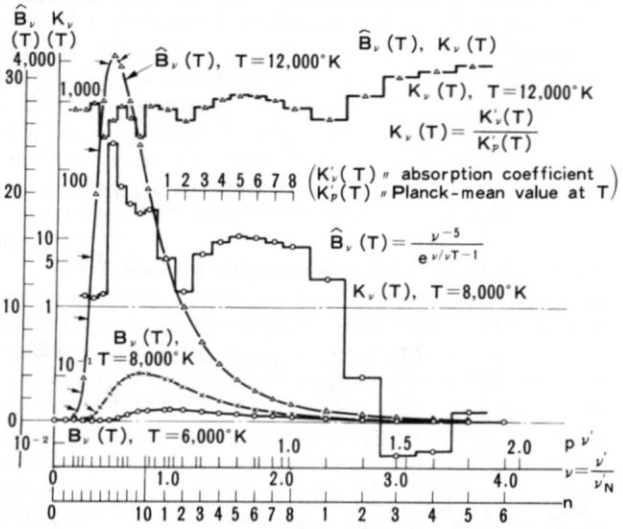

Fig. 10 Radiation Characteristic of Nongrey Gas

III. Optimum Shape

3.1 Introduction

In the previous chapter, we have discussed aerodynamic heat transfer in relation to the geometry of vehicles from the view point of rarefied gasdynamics and of hypersonic boundary layer analysis. In this chapter, by utilizing those results, we proceed to the optimization problem of minimizing the total heat transfer rate to a vehicle. It is known that total heat transfer rate is widely different depending upon the angle of attack ranged between 0 to 90°, and thus it can hardly be expected to exist some optimum vehicle geometry irrespective of its attitude. Therefore, it would rather be pertinent to bring up a problem of optimum vehicle geometry of minimum total heat transfer rate at a given angle of attack than to discuss that mentioned above. In the following, the optimum geometries are investigated for the axially symmetric body of given volume and base diameter and for the two-dimensional supersonic wing profile of given lift coefficient and cross sectional area.

Essentially, the optimization of the aerodynamic heating during the reentry phase should involve both problems of vehicle geometry and of flight trajectory, and thus the investigation introduced here would be regarded as the first step for the solution of the combined field.

3.2 Rarefied gas flow

Total heat transfer rate for the hemisphere-cylinder is also calculated and compared with that of the sharp cone of equal volume and base diameter as is shown in Fig. 11. For small angle of attack, heat transfer to the cone is less than that of the hemisphere-cylinder. But for large angle of attack, on the contrary, the hemisphere-cylinder becomes preferable.

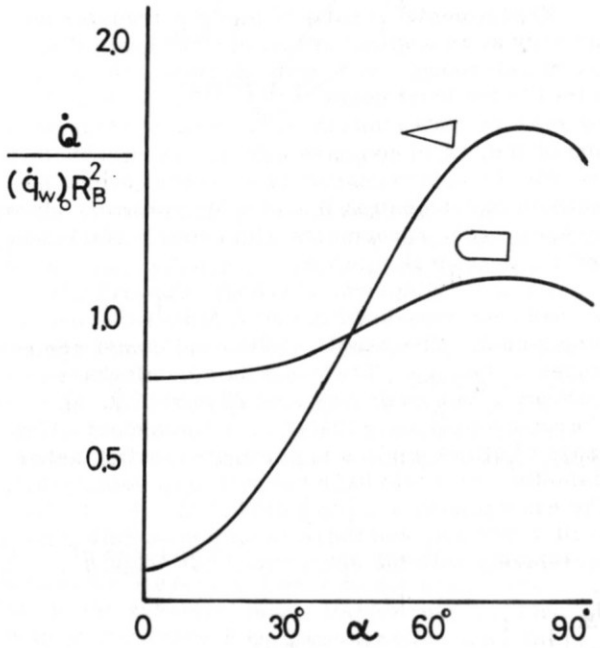

Fig. 11 Total heat transfer rate for the sharp cone and hemisphere-cylinder

One of the authors obtained the optimum shape for axially symmetric body under the condition that its volume and base diameter are given constants, in the case of continuum hypersonic flow at zero incidence.[17][18] Here in rarefied flow regime, we discuss the optimum shape for given angle of attack under the same condition mentioned above.

Cylindrical coordinates system (x, y, ϕ) shown in Fig. 12, is used. Let θ be the angle between the surface normal at the stagnation line ($\phi = 0$) and the body axis, then ψ is written as follows;

$$\cos\psi = \cos\alpha\cos\theta + \sin\alpha\sin\theta\cos\phi \qquad (3.1)$$

The problem is to minimize

$$\frac{\dot{Q}}{(\dot{q}_w)_0} = \int_0^L\int_0^{\phi_0} y(\cos\alpha\cos\theta + \sin\alpha\sin\theta\cos\phi)^3 \cdot \sec\theta\, dx\, d\phi \qquad (3.2)$$

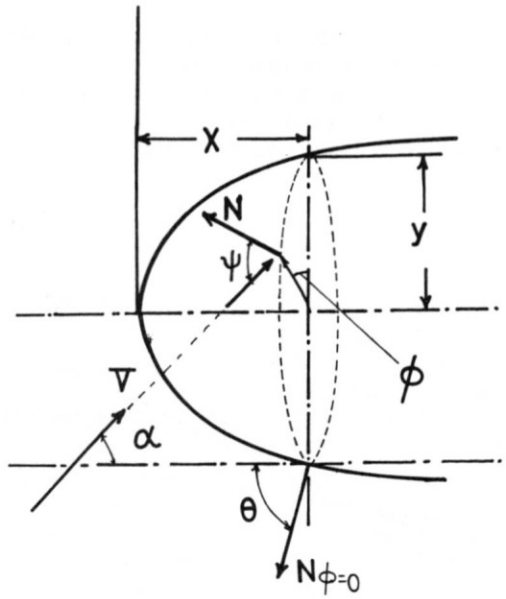

Fig. 12 Coordinate system

under the constraint

$$V = \pi \int_0^L y^2 dx = \text{given constant} \tag{3.3}$$

where L is the body length, and

$$\phi_{iu} = \frac{\pi}{2} + \sin^{-1} t \qquad \text{for } t \leqq 1 \tag{3.4}$$

$$\phi_u = \pi \qquad \text{for } t > 1 \tag{3.5}$$

$$t = \cot\alpha \cot\theta \tag{3.6}$$

Euler equation derived from variational calculus is solved into

$$\frac{(\cot^2\alpha + 3t^2)}{(\cot^2\alpha + t^2)^2}\left\{\left(\frac{\pi}{2} + \sin^{-1} t\right)\left(t^2 + \frac{3}{2}t\right) + \left(\frac{11}{6}t^2 + \frac{2}{3}\right)\sqrt{1-t^2}\right\}$$

$$-\frac{1}{(\cot^2\alpha + t^2)}\left\{\left(\frac{\pi}{2} + \sin^{-1} t\right)\left(3t^3 + \frac{3}{2}t\right) + \frac{9}{2}t^2\sqrt{1-t^2}\right\}$$

$$= \lambda y \qquad \text{for } t \leqq 1 \tag{3.7}$$

$$\frac{\pi(3 - 2\cot^2\alpha)t^3}{(\cot^2\alpha + t^2)^2} = \lambda y \qquad t > 1 \tag{3.8}$$

where the integral constant is already determined by assuming the curve intersects t-axis (y=0), and λ is Lagrange's multiplyer. For given V, λ is determined from

$$\frac{V}{\pi} = \int_0^{R_B} \frac{y^2 dy}{\cot\theta} \tag{3.9}$$

where R_B is the radius at the base and t_0 and t_λ are values of t when $\lambda y = 0$ and $\lambda y = \lambda R$ respectively. Once λ is determined, Eqs. (3.7), (3.8) and

$$x = \int_0^y \frac{dy}{\cot\theta} \tag{3.10}$$

give the geometry of optimum shape. By putting $t = t_\lambda$ in Eq. (3.10), L is also determined. In Figs.

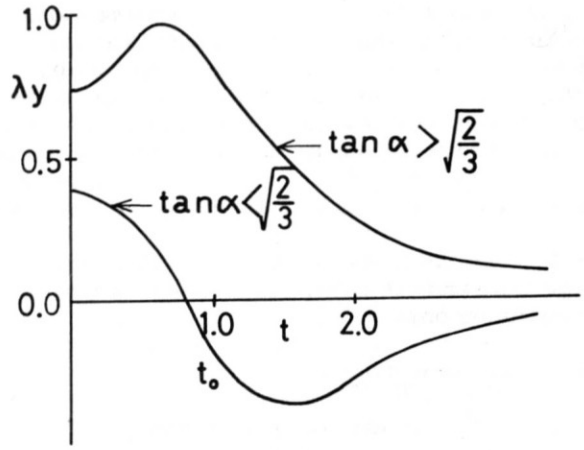

Fig. 13 a) Variation of solution due to the angle of attack
The curves of Eqs. (3.7) and (3.8)

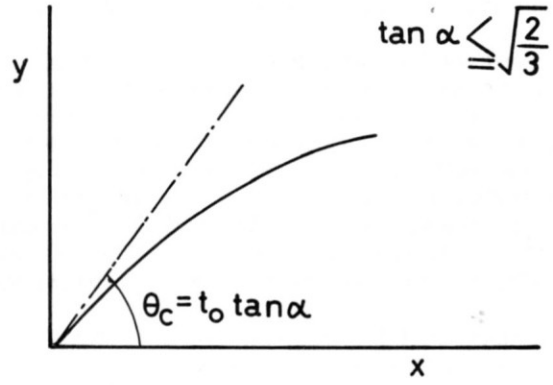

Fig. 13 b) Variation of solution due to the angle of attack
The optimum shape for $\tan\alpha \leqq \sqrt{\frac{2}{3}}$

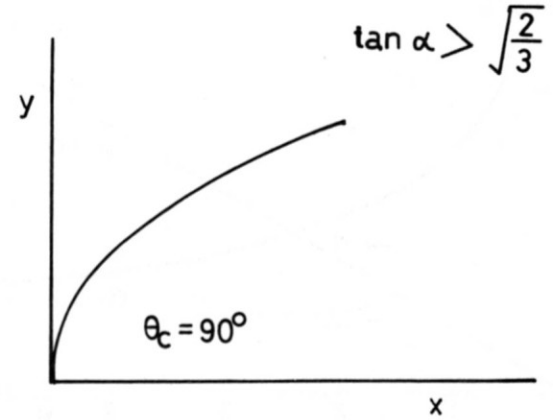

Fig. 13 c) Variation of solution due to the angle of attack
The optimum shape for $\tan\alpha > \sqrt{\frac{2}{3}}$

13a, 13b and 13c, how the solution curve varies with the angle of attack, is displayed. For tan $\alpha < \sqrt{\frac{2}{3}}$ ($\alpha = 39°$ approximately) t_0 lies between 0 and 1. In this case optimum shape has sharp nose and the semi-vertex angle of which increases with increasing angle of attack from zero to its maximum value of 39°. For tan $\alpha > \sqrt{\frac{2}{3}}$, t_0 becomes infinite. In this range of attack angle, optimum shape has blunt nose.

By calculating the second variation numerically, we can verify that these solutions correspond to the minimum ones.

3.3 Hypersonic flow

As in the previous section for rarefied flow, the optimum shape can be calculated for steady hypersonic flow. For the zero angle of attack, one of the present authors studied this problem by the more precise method (18)(17). The minimum heat transfer body with given fineess ratio was shown in Ref. 17, but the sharp cone solution for given volume and base diameter was only mentioned in Ref. 18.

However the similar problem about arbitrary angle of attack, even we assume that (2.6) is valid for general axially symmetric body, must be solved by numerically. In this section we consider only the combination of spherical nose or sharp cone and cylindrical body. For the body without angle of attack, the results by (2.6) show similar tendency with Aihara's solution(18). The total heat transfer for the sharp cone decreases with increasing volume.

Contrary at $\alpha = 90°$, the total heat transfer increases with increasing volume. We show these results in Fig. 14 about nondimensional total heat transfer rate $\dot{Q}/(\dot{q}_w)_0 R_0^{\frac{1}{2}} R_B^{\frac{3}{2}}$. We also show the values for the hemisphere at $\alpha = 0$ and $\alpha = 90°$.

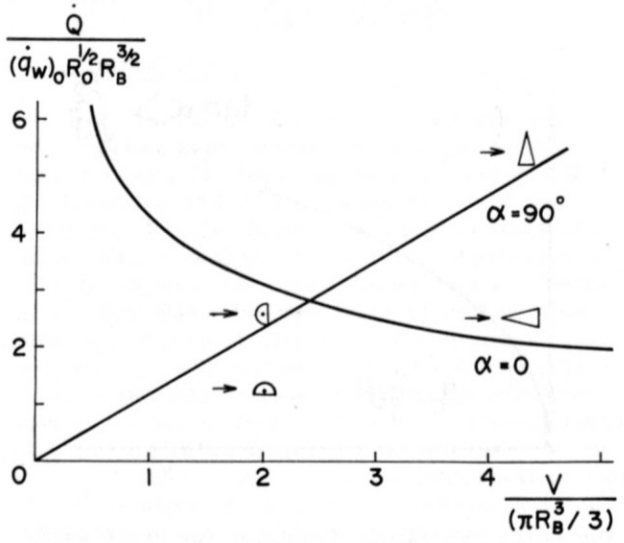

Fig. 14 Calculated nondimensional total heat transfer ratio at $\alpha = 0$ and 90° vs. volume of sharp cone with given base diameter

Complete calculation for arbitary shape and attack angle is not yet finished, we only show an example about the one, the cone-cylinder and hemisphere-cylinder with equal volume and base diameter (Fig.15). At large angle of attack, the hemisphere-cylinder is preferable for heat transfer.

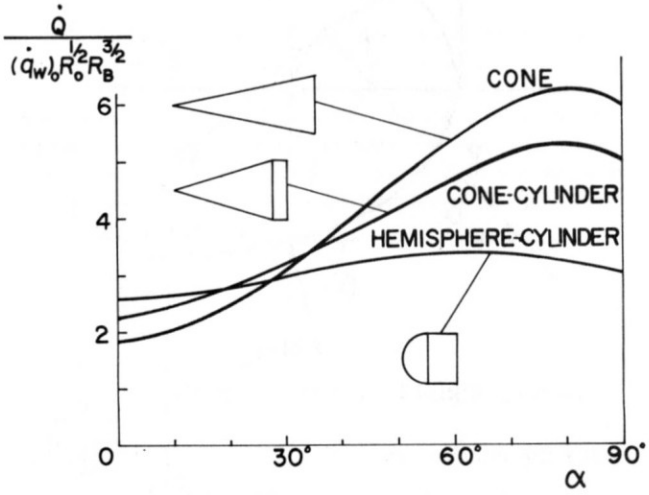

Fig. 15 Calculated value of total heat transfer ratio of cone, cone-cylinder, and himisphere-cylinder with equal volume and base diameter for various angles of attack

3.4 Two-dimensional Wing Section

In this section we treat the problem of minimizing the total heat transfer of two-dimensional wings in supersonic flow.

Consider a two-dimensional airfoil at zero angle of attack, and denote by x a coordinate in the flow direction and by y a coordinate perpendicular to x. By setting the chord length equal to 1, we can express the integral to be minimized as(17)

$$I = \sum_{j=u,\ell} \int_0^1 \frac{\rho_{ej}}{\rho_0} \frac{u_{ei}}{u_\infty} \left[1 + \left(\frac{dy}{dx} \right)_j^2 \right] dx \qquad (3.11)$$

where the subscript j refers to the upper surface (u) or the lower surface (l), and the subscripts e, o, and ∞ refer to local boundary layer edge, stagnation, and infinity, respectively. We impose two constraints on this optimal problem:

(1) lift coefficient C_L is given, and
(2) cross sectional area S is given.

The lift coefficient at zero angle of attack which results from second-order analysis is

$$C_L = \frac{(M_\infty^2 - 2)^2 + \gamma M_\infty^4}{2 (M_\infty^2 - 1)^2} \int_0^1 \left(\left(\frac{dy}{dx} \right)_\ell^2 - \left(\frac{dy}{dx} \right)_u^2 \right) dx \qquad (3.12)$$

where M_∞ is Mach number, while the cross sectional area is given as

$$S = \int_0^1 (y_u - y_\ell)\, dx \qquad (3.13)$$

By employing terms up to second order in dy/dx, we can express p and u as follows:

$$\frac{p_{e_j}}{} = \frac{1}{2}\gamma p_\infty M_\infty^2\left[\pm\frac{2}{\sqrt{M_\infty^2-1}}\left(\frac{dy}{dx}\right)_j + \frac{(M_\infty^2-2)^2+\gamma M_\infty^4}{2(M_\infty^2-1)^2}\left(\frac{dy}{dx}\right)_j^2\right] \quad (3.14)$$

$$u_{e_j} = \left[\frac{2\gamma}{\gamma-1}\frac{p_0}{\rho_0}\left(1-\left(\frac{p_{e_j}}{p_0}\right)^{\frac{\gamma-1}{\gamma}}\right)\right]^{\frac{1}{2}} \quad (3.15)$$

By specifying C_L , S, and M_∞ we can formulate a conditional variation problem in general. In the following, however, we restrict ourselves to double-wedge profiles which are already known to be the optimum profile of minimum wave drag. If Reynolds analogy can be extended to the behavior of the boundary layer along a double-wedge wing, the optimum profile obtained in this study may also be regarded as a favourable one from the view point of total drag.

In the case of double-wedge wing, the variables are upper and lower thicknesses of the wedge, y_U and y_L , and their chordwise positions, x_U and x_L . By specifying C_L and S we can eliminate former two variables, and thus can integrate Eq. (3.11) to find a minimum value by changing x_L for a given x_U , 0.1, 0.2, ... , and 0.9.

Numerical calculations are performed for C_L = 0.1, S=0.05, and M_∞=5, 7, and 10, and it is found that there is a general tendency that the total heat transfer rate is small when $x_L = x_U$ or $x_L = 1-x_U$. Among these wings the optimum wing profile which is irrespective of Mach number is found to have the following dimensions:
$x_U = x_L$ = 0.8 or 0.2 and y_U = -0.0162 and y_L = -0.1162. The Profile is shown in Fig. 16. The changes of the total heat transfer rate with the change of the location of x_U and x_L 0.7 or 0.3 holding y_U and y_L at the same values are about 4, 5 and 6% for M_∞ = 5, 7 and 10, respectively.

The more detailed considerations such as the excess of heat transfer at the corner as pointed out by Zakkay and Tani [12] are not involved in this analysis and further improvements are to be made on such points.

Fig. 16 Optimum double-wedge profile of minimum heat transfer of given lift coefficient and cross sectional area

IV. Aerodynamical Characteristics of Winged Vehicle

4.1 Objects of present study

At the reentry flight, as shown in Fig. 1, the space shuttle through the wide range of flight condition. In this report, we research the optimum problem for heat transfer at rarefied regime and high Mach number flight, so we mainly consider aerodynamic characteristics in these flight conditions. Optimum shape and optimum trajectory concern to each other, and depend on the heat transfer distribution and also on the aerodynamic characteristics. In this report, we consider these effects separately as follows:

(1) Body shape is determined by heat transfer characteristics at rarefied flow and hypersonic flight.
(2) Wing is determined by supersonic flight condition, because wing is necessary in dense atmosphere. Its profile is given in 3.4, and plan form is considered for given body shape.
(3) Aerodynamic characteristics of complete configuration are offered for optimum flight calculation.

In this chapter, we will consider these problems in each speed regime.

4.2 Hypersonic flow -- Newtonian theory

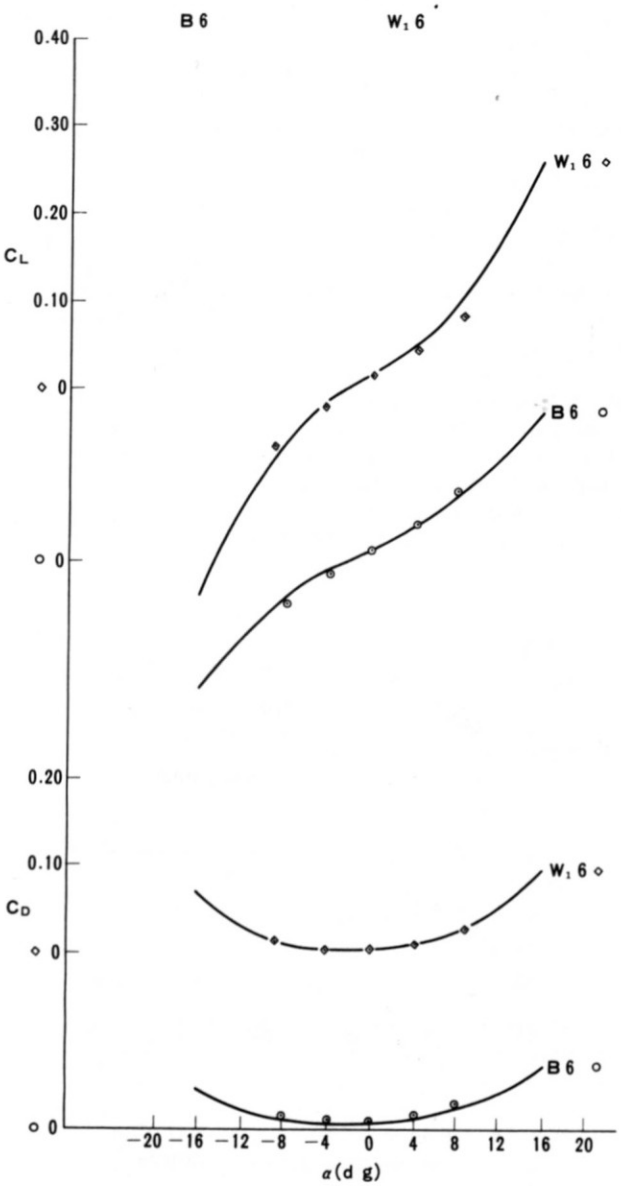

Fig. 17 Aerodynamic Characteristics of Halfcone, — Newtonian Flow Analysis

As mentioned in 2.2 and 2.4, the aerodynamic characteristics of vehicle in low density atmosphere and at hypersonic flight can be estimated by the Newtonian flow approximation. The explicit forms of the aerodynamic forces are given in text books (for an example, Ref. 19). We have a computer program for this calculation about arbitary three-dimensional body shape, and here we show an example calculated by this program for the half cone (Fig. 17).

4.3 Supersonic flow

In this section we consider aerodynamic characteristics at supersonic flight for given bodies, which are determined by heat transfer consideration. We chose cylindrical bodies with two types of nose, sharp cone for small attack angle reentry and hemisphere for high attack angle reentry.

As supersonic flight both configurations fly only with small angle of attack. So we can apply the linearized potential flow theory for sharp cone cylinder with flat plate wings. However the supersonic flow around the spherical nose cylinder can not be treated by potential flow because of the existence of the strong bow shock wave.

We have continued the study about aerodynamics of blunt body theoretically and also experimentally at the supersonic wind tunnel of N. A. L. The drag force of the blunt nosed body can be estimated by the Newtonian flow even for moderate supersonic flow, but can not for the normal force on the blunt body (Fig. 18) [20].

The shear layer around cylindrical body caused by bow shock wave was treated numerically and experimentally (Fig. 19) [21]. The effect of this layer on the wing was measured for rectangular wings with various span length (Figs. 20, 21). This effect can be estimated by non-uniform Newtonian flow approximation for shear layer flow.

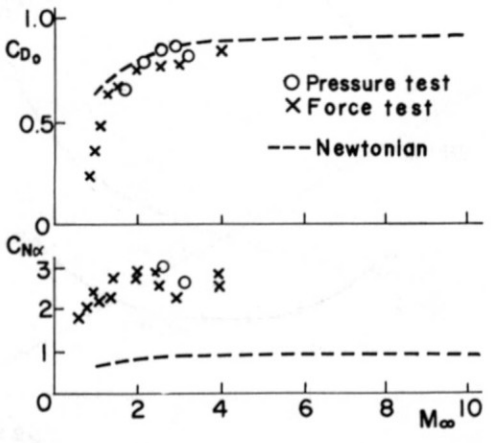

Fig. 18 Coefficients of pressure drag and normal force of hemisphere-cylinder

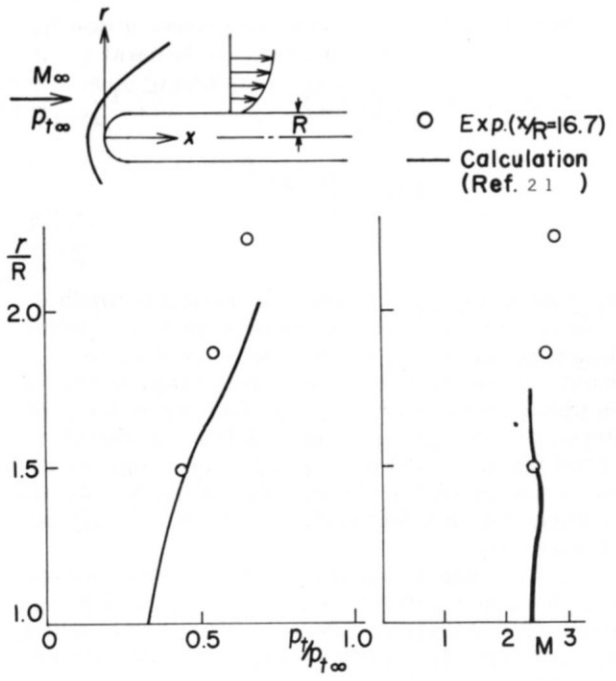

Fig. 19 Shear layer profile around spherical nose cylinder at $M_\infty = 3$

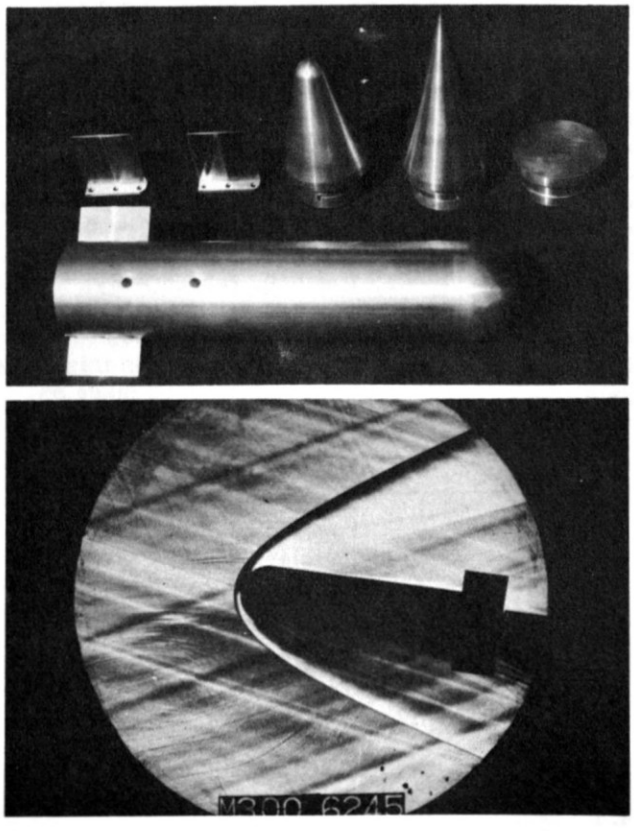

Fig. 20 Force test model of N. A. L. supersonic wind tunnel with various noses and wings

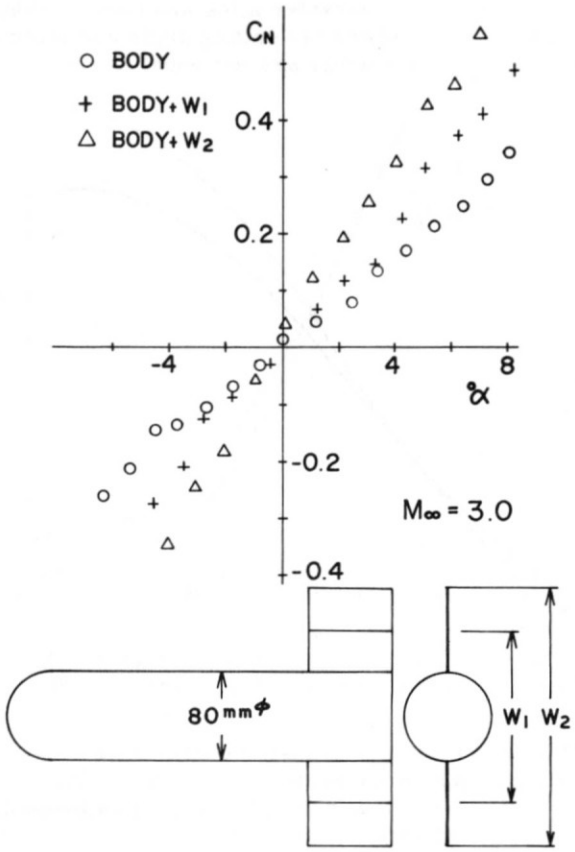

Fig. 21 Normal force of hemisphere-cylinder with various wings

4.4 Miscellaneous problems

Concerning to the aerodynamic characteristics of space shuttle we have to consider many other problems. The separation of the orbiter and the boosters is one of the important problems. The interaction between multi bodies is also estimated by the non-uniform Newtonian flow approximation (22).

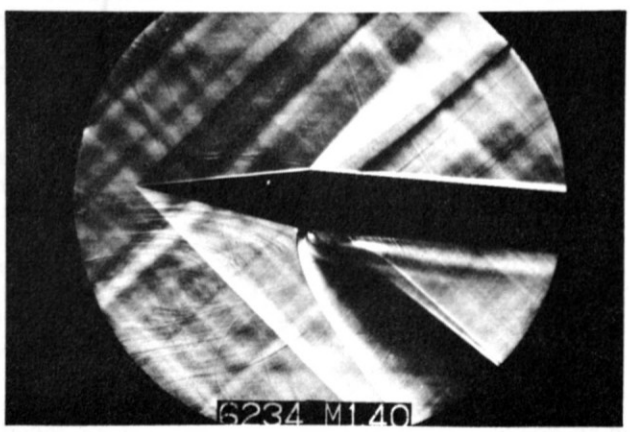

Fig. 22 Side jet ejection in N. A. L. supersonic wind tunnel

The attitude control in rarefied atmosphere shall be done by the side jet ejection, but these control must be used carefully in dense atmosphere. The effects of ejected side jet on the afterbody or on the wing have been studied experimentally in the supersonic and transonic wind tunnels of N. A. L. (Fig. 22).

Aerodynamic problems at low speed flight are not considered in this report.

V. Optimum Trajectory

5.1 Introduction

In space-flight problems one of the most serious matters is to find some means of reducing the tremendous amount of aerodynamic heat transfer to a vehicle in the reentry stage.

In this chapter we extend the previous work (1) to the optimum reentry trajectory of minimum heat transfer to a lifting vehicle with a retromotor by making use of the results obtained in previous chapters. This problem is particularly important in relation to our interest in the feasibility of developing a reusable space transportation system.

Here we focus our attention to total convective heat transfer to the vehicle during reentry which is considered to be the dominating cause of heating in the present problem.

The present investigation is undertaken in an attempt to discuss two reentry vehicles with different nose shapes, that is, a sharp cone-cylinder and a hemisphere-cylinder with lifting wings.

5.2 Fundamental equations

The augmented function for the conditional variation principle is

$$F = \dot{Q} + \sum_{i=1}^{5} \lambda_i \varphi_i \qquad (5.1)$$

where

$$\dot{Q} = \int \dot{q}_w \, dS$$

$$\varphi_1 = \dot{x} - V\cos\gamma$$

$$\varphi_2 = \dot{z} - V\sin\gamma$$

$$\varphi_3 = M\dot{V} + Mg_*\left(\frac{z_*}{z}\right)^2\sin\gamma + g_*\left(\frac{1}{2}\rho V^2\pi R_B^2 C_D - c\beta\cos\psi\right)$$

$$\varphi_4 = MV\dot{\gamma} - Mg_*\left(\left(\frac{V}{V_c}\right)^2\frac{z_*}{z} - \left(\frac{z_*}{z}\right)^2\right)\cos\gamma - g_*\left(\frac{1}{2}\rho V^2\pi R_B^2 C_L + c\beta\sin\psi\right)$$

$$\varphi_5 = M + \beta$$

and λ_i's are Lagrange multipliers. Dott means differentiation with respect to time. The coordinate system is shown in Fig. 23. In Eq. (5.1), $\dot{Q}$ means the total heat transfer rate to the vehicle while in the previous work the heat transfer rate at the stagnation point was discussed. Standard atmospheric table is used for evaluating air density ρ.

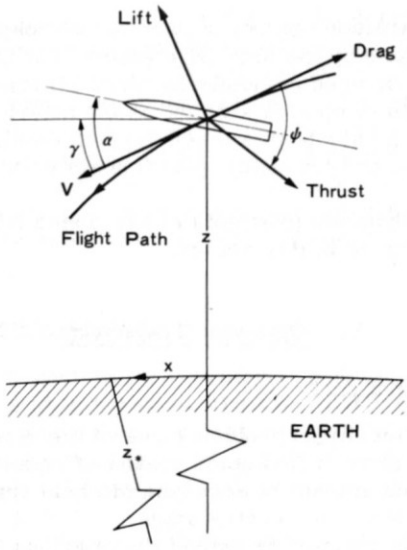

Fig. 23 Coordinate system

State variable in Eq. (5.1) are x, z, V, , and M and control variables are α, β, and ψ. The Euler-Lagrange equations are derived as usual way from Eq. (5.1). Reentry duration, surface range and the altitude at final time are unspecified but the final speed is set equal to 3 km/sec in relation to the validity of Newtonian flow assumption in this calculation, so the same transversality condition for the variation used in Ref. 1 is again introduced. Eliminating Lagrange multipliers and some variables by utilizing Euler-Lagrange equations and the transversality condition with a lengthy but rather straightforward calculation, we can reduce our optimization problem to a system of differential equations with four parameters, V, γ, α, and ψ, which is solved numerically by Runge-Kutta -Gill method with a time interval of 0.5 sec.

5.3 Numerical examples

Numerical calculations are carried out for the following two vehicles: (1) sharp conecylinder with rectangular flat plate middle wings and a retromotor, and (2) hemisphere-cylinder with rectangular flat plate middle wings and a retromotor. The dimensions of these vehicles are shown in Table 1 and total heat transfer coefficients of the fuselages*

	Nose length	Cylinder length	Volume	Wing chord length	Wing span length
(1)	$5\ R_B$	$8\ R_B$	$\frac{29}{3}\pi R_B^3$	$1.5\ R_B$	$8\ R_B$
(2)	R_B	$9\ R_B$	$\frac{29}{3}\pi R_B^3$	$1.5\ R_B$	$8\ R_B$

Table 1. Dimensions of the vehicles (R_B = Radius of cylinder)

and aerodynamic characteristics are shown in Figs. 24, 25, and 26, where the setting angle and the dihedral angle of the wings are set equal to zero.

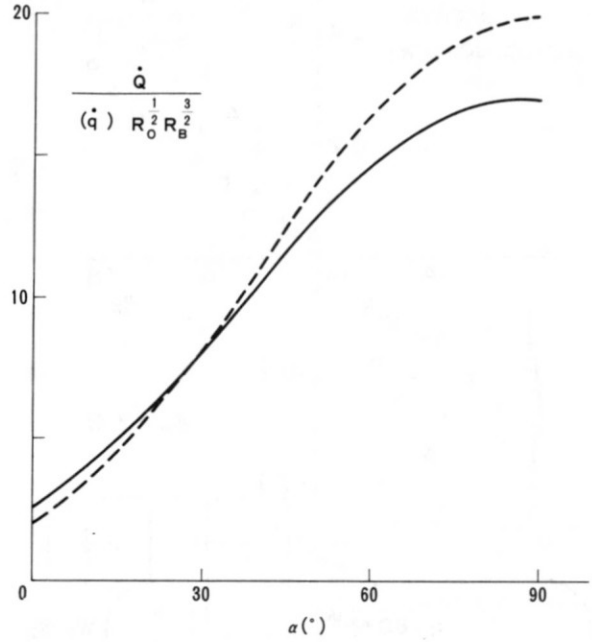

Fig. 24 Total heat transfer coefficients of the fuselages vs. α
---- sharp conecylinder, — hemisphere-cylinder

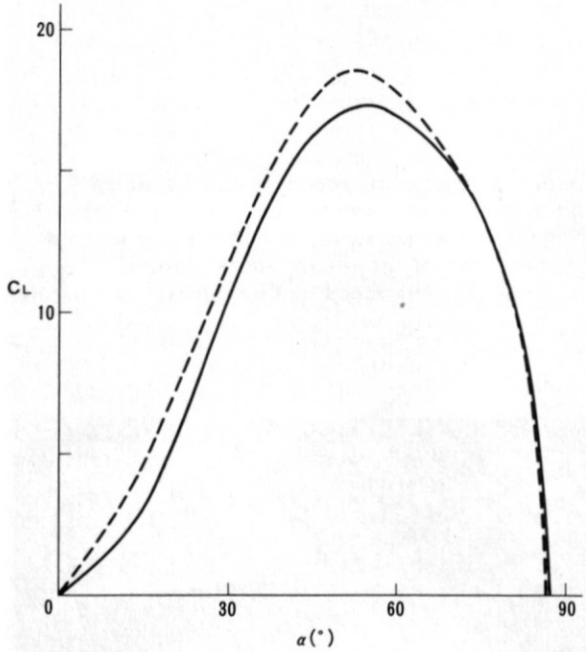

Fig. 25 Lift coefficients of the vehicles vs. α
---- sharp conecylinder, — hemisphere-cylinder

* Heat transfer coefficient of the wings is obtained by Newtonian flow analysis to be $9\sin^3\alpha$ for the present case and is added to the data in Fig. 24 when numercial calculations are performed.

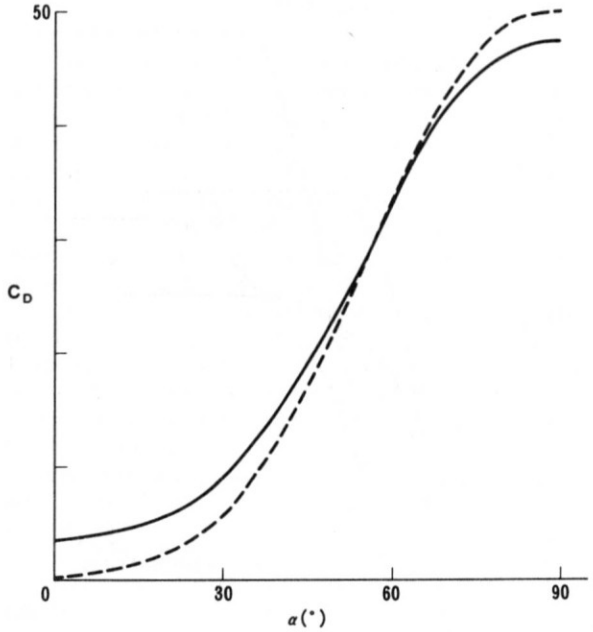

Fig. 26 Drag coefficients of the vehicles vs. α
---- sharp conecylinder, — hemisphere-cylinder

Numerical constants and initial conditions are set as follows:
$g_* = 9.8\,m/sec^2$, $R = 1\,m$, $c = 3\times10^3$ m/sec, $\beta = 1.46\,kg/sec$ $x(0) = 0$, $z(0) - z_* = 1.2\times10^5$ m, $V(0) = 1.1\times10^4$ m/sec, $M(0) = 7.3\times10^3$ kg, $\alpha(0) = 90°$, $\alpha(0) = -5°, -10°$, where optimum $\psi(0)$ is determined from the Euler-Lagrange equations and other initial conditions. It should be emphasized that the trajectories obtained in the next section are therefore considered to be optimum under the given conditions as stated above.

5.4 Results and discussion

Numerical results are shown in Figs. 24-31. In each figure, broken lines and solid lines show the results for the sharp conecylinder and the hemisphere-cylinder, respectively.

As can be seen in Fig. 27, the optimum reentry trajectories are initially almost straight and then show a tendency to make the inclination of the flight paths to the horizon deeper.

Numbers plotted along the trajectories represent the flight time in second elapsed after the reentry. It is noticed that for the hemisphere-cylinder the vehicle changes its attitude form 90° to 0 at almost the same altitude irrespective of $\gamma(0)$ on referring to Fig. 28 which shows the optimum operations during the reentry. As for the sharp conecylinder, it keeps α constant at 90° and this is the distinct contrast to the behavior of the hemisphere-cylinder.

At the final stage, the trajectories are characterized by skipping phase during which the vehicles make use of gravity component and the retromotor so as to reduce the velocity and the same kind of feature is already obtained in Ref. 1.

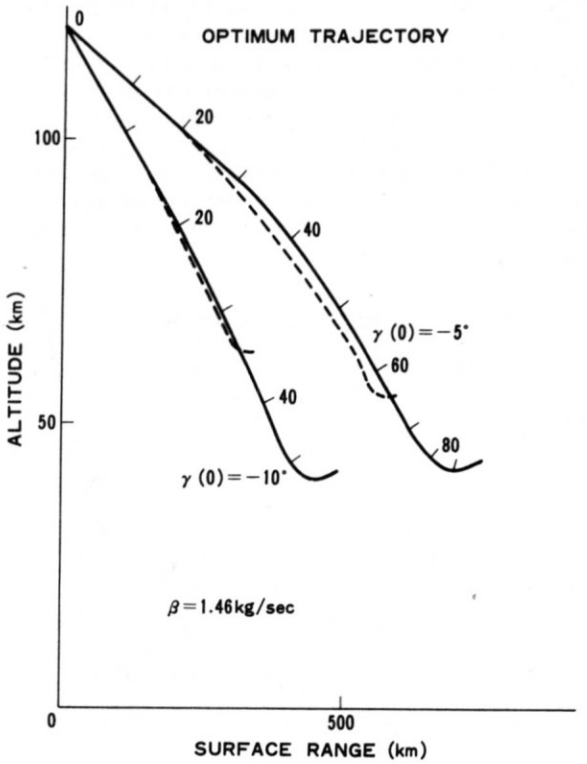

Fig. 27 Optimum reentry trajectories for $\gamma(0) = -5°, -10°$
---- sharp conecylinder, — hemisphere-cylinder

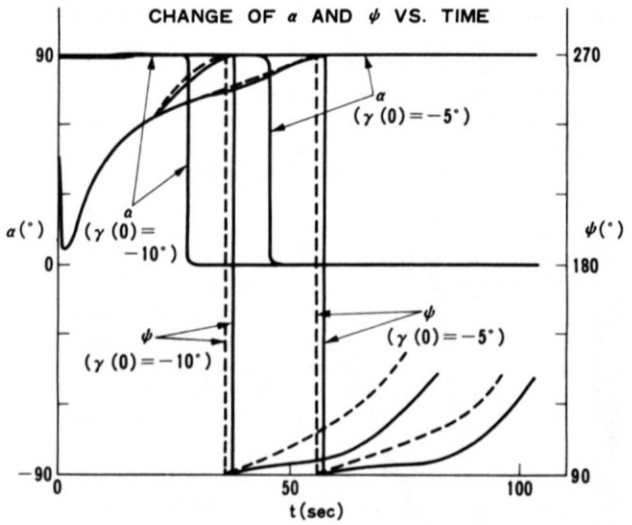

Fig. 28 Change of attack angle and thrust direction angle vs. time for $\gamma(0) = -5°, -10°$
--- sharp conecylinder, — hemisphere-cylinder

The variation of velocity vs. time is shown in Fig. 29. The variation along each trajectory for the hemisphere-cylinder is almost the same above 80 km or below 50 km in altitude but it shows respective characteristic deceleration in between.

It is noticed that those behaviors are strongly related to the control of the vehicles as shown in Fig. 28. The sharp conecylinder is seen to be decelerated more rapidly without any characteristic feature. The maximum decceleration is seen to occur in the denser atmosphere of lower altitude.

Interesting features of heat transfer are observed from Figs. 30 and 31 where the ordinates are not dimensional but express the relative magnitude.

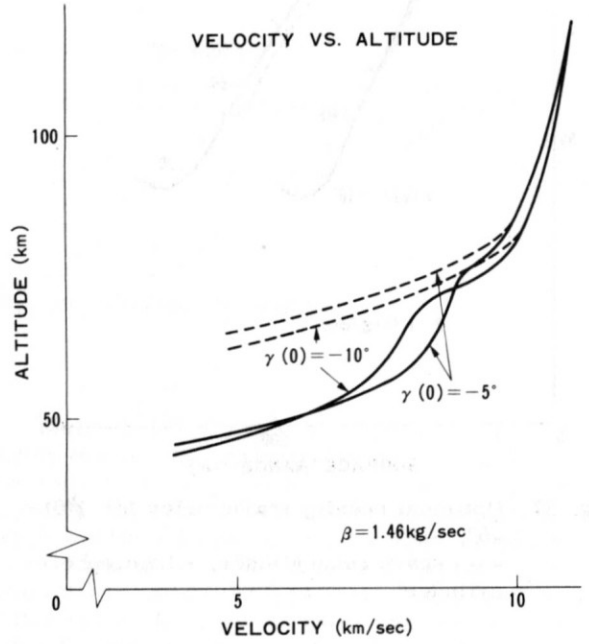

Fig. 29 Velocity vs. altitude along trajectories for $\gamma(0)$ = -5°, -10°
--- sharp conecylinder, — hemisphere-cylinder

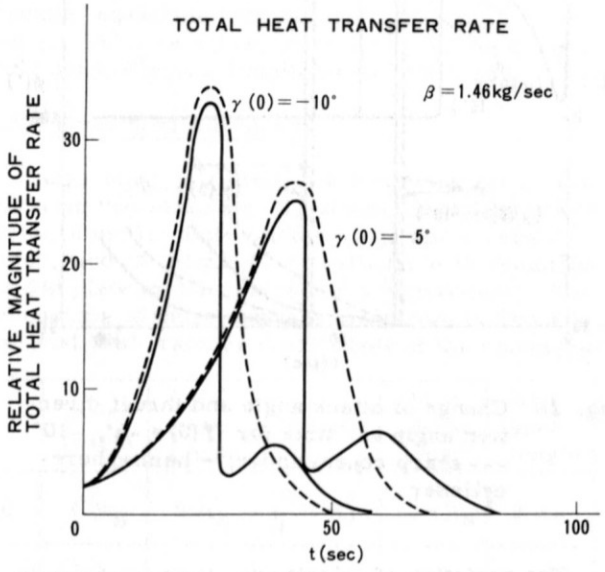

Fig. 30 Relative magnitude of total heat transfer rate vs. time for $\gamma(0)$ = -5°, -10°
--- sharp conecylinder, — hemisphere-cylinder

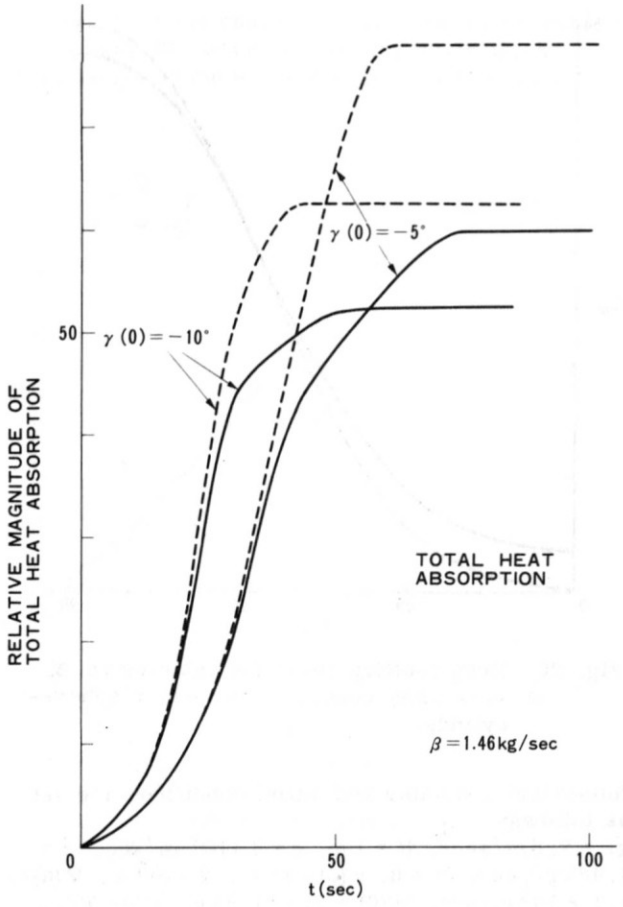

Fig. 31 Relative magnitude of total heat absorption vs. time for $\gamma(0)$ = -5°, -10°
--- sharp conecylinder, — hemisphere-cylinder

The maximum value of the heat transfer rate is small for shallow reentry, but as for the total heat absorption, the shallow reentry is, on the contrary, disadvantageous owing to its longer duration. Therefore, for each vehicle, $\gamma(0)$ should be chosen in relation to the decision of the aim of optimization and to some permitted limit of instantaneous heat flux to the vehicles. The reduction of total heat transfer rate from its maximum to extremely lower value is achieved by alining the vehicle to the flight direction for the hemisphere-cylinder and by the larger rate of deceleration for the sharp conecylinder. The second excess of total heat transfer rate for the hemisphere-cylinder is not too serious and overcome by the deceleration of flight velocity (Fig. 30).

Through Figs. 30 and 31, as far as we are concerned with the data used in the analysis, it is concluded that the hemisphere-cylinder is more advantageous than the sharp conecylinder in instantaneous heat transfer rate as well as its integrated value.

VI. Conclusions

A space shuttle, an unmanned lifting body combined with reusable boosters is proposed. Reentry trajectory of a lifting body covers a wide range of aerodynamics. The enormous heat input during the reentry stage is the most serious problem for the structural design of the lifting body.

One can reduce the total heat input of the reentry flight either by taking the optimum trajectory or by forming the optimum shape.

Application of lifting capability the reentry vehicle can take the optimum path to minimize the heat input during the flight. The problem can be solved by means of the optimization technique that is either by the classical variational principle or by the Pontryagin's maximum principle. In the course of reentry flight the optimum trajectory can be frequently achieved by incleasing the angle of incidence of the body to the main flow direction.

Therefore the aerodynamic heating of the blunt or sharp nosed cylinder is studied. The theoretical results are checked by experimental data for several cases. The heat input analysis has been conducted mostly in the region of hypersonic speed and sometimes of supersonic speed, since most of the trajectory belongs to those speed ranges. The effect of radiation is also considered for the extreme speed.

The optimum shape should be determined to reduce the maximum heat input at the stagnation or the total heat input on the whole surface of the body. In the present study, the reduction of the overall heat input introduces the objective function. The optimum path for the lifting body is carried out on the computer. The application of a retro rocket or a control jet is sometimes effective to extend the range of the optimum flight.

The structure of the problem of the optimization is indicated in the Fig. 32. Assuming the lifting capability the optimum trajectory is determined. From the optimum trajectory, the angles of attack for various flight conditions are found. The heat input analysis for each angle of attack is then introduced to determine the optimum shape. The shape of the body determines the aerodynamic characteristics of the body. Accordingly the problem consists of a closed loop which could be solved by means of iteration.

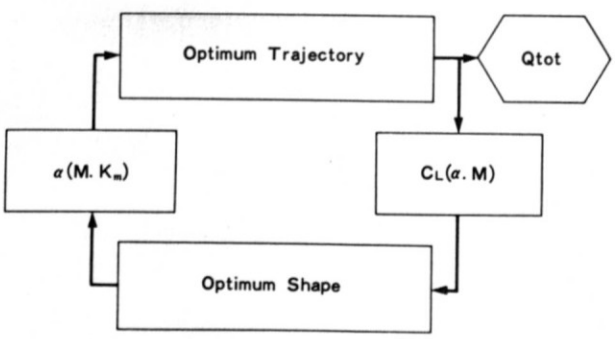

Fig. 32 Structure of the problem of the optimization

References

1. Kondo, J. and Aihara, Y., "The Optimum Reentry Trajectory of A Lifting Vehicle," Proc. Ninth Int. Symp. Tech. Sci., Tokyo, 1971, pp. 265-272.
2. Chow, R., "Stagnation Point Heat Transfer of a Blunt-Nosed Body in Low-Density Flow," AIAA J. Vol. 1, No. 5, 1963 pp. 1220-1222.
3. Potter, J. L., "The Transitional Rarefied-Flow Regime," Rarefied Gas Dynamics, Academic Press, 1966, pp. 881-937.
4. Collis, D. C. and Williams, M. J., "Two-dimensional Convection from Heated Wires at Low Reynolds Numbers," J. Fluid Mech. 6, 1959, pp. 357-384.
5. Aihara, Y., Kassory, D. R., and Libby, P. A., "Heat Transfer from Circular Cylinders at Low Reynolds Numbers. II. Experimental Results and Comparison with Theory," Phys. Fluids 10, 1967, pp. 947-952.
6. Levey, H. C., "Heat Transfer in Slip Flow at Low Reynolds Numbers," J. Fluid Mech. 6, 1959, pp. 385-391.
7. Kassoy, D. R., "Heat Transfer from Circular Cylinders at Low Reynolds Numbers. I. Theory for Variable Property Flow," Phys. Fluids 10, 1967, pp. 938-946.
8. Stadler, J. R., Goodwin, G., and Creager, M. O., "Heat Transfer to Bodies in a High Speed Rarefied Gas Stream," NACA TN 2438, 1951.
9. Lees, L., "Laminar Heat Transfer Over Blunt Nosed Bodies at Hypersonic Flight Speeds", Jet Populsion, Vol. 26, 1956, pp. 259-269.
10. Reshotko, Eli and Beckwith, I. E., "Compressible Laminar Boundary Layer over a Yawed Infinite Cylinder with Heat Transfer and Arbitary Prandtl Number", NACA Report 1379, 1958.
11. Conti, R. J., "Laminar Heat-Transfer and Pressure Measurements at a Mach Number of 6 on Sharp and Blunt 15° Half-angle Cones at Angles of Attack up to 90°", NASA Technical Note D-962, Oct. 1961.
12. Zakkay, V. and Tani, T., "Theoretical and Experimental Investigation of the Laminar Heat Transfer Downstream of a Sharp Corner", Proc. IV Congress of Applied Mech., Mech., Vol. 4, pp. 1455-1467.
13. Bushnell, D. M., Jones, R. A. and Huffman, J. K., "Heat-Transfer and Pressure Distributions on Spherically Blunted 25° Half-angle Cone at Mach 8 and Angles of Attack up to 90°", NASA Technical Note D-4792, Oct. 1968.
14. De Jarnette, F. R. and Davis, R. M., "A Simplified Method for Calculating Laminar Heat Transfer over Bodies at an Angle of Attack", NASA Technical Note D-4720, Aug. 1968.
15. Kondo, J., Tamaki, F., Kawamura, R. and Kamimoto, G., "Recent Progress of the Re-Entry Aerodynamics Research in Japan", Aerospace Proceedings 1966, pp. 627-662.

16. Kondo, J., "Radiation in Stagnation Flow Region," 22nd Congress of the International Astronautical Federation, Brussels, 1971.
17. Aihara, Y., "Optimum Body Geometries of Minimum Heat Transfer at Hypersonic Speeds", AIAA Journal, Vol. 6, 11, 1968 pp. 2187-2189.
18. Aihara, Y., "Minimum Heat Transfer Body at Hypersonic Speeds", Tech. Report of N. A. L. TR-151, 1968 (in Japanese).
19. Truitt, R. W., "Hypersonic Aerodynamics", Ronald Press, New York 1959, Chapt. 8.
20. Kawamoto, I., "Some Considerations on the Aerodynamic Characteristics for the Body of a Rocket with Blunt Nose", The report of N. A. L. TR-266, 1972 (in Japanese).
21. Kawamoto, I., "Supersonic Flow Fields around a Cylindrical Body with Blunt Nose", The Report of N. A. L. TR-199 1970 (in Japanese).
22. Kondo, J., Tani, T. and Kawamoto, I., "Interaction of Bodies in Supersonic Flow", Preprint of 2nd meeting of Fluid Dyn., Tokyo 1970 (in Japanese).